VR Ocean

Real-Time Ocean Surface Synthesis via Inverse FFT with Vectorized Job Parallelism and Adaptive Quadtree Level-of-Detail for Virtual Reality

Roman Aebi

Contents

Abstract

This work presents a real-time ocean simulation system optimized for virtual reality applications. The implementation combines Fast Fourier Transform (FFT) based wave synthesis using the Phillips spectrum with an adaptive quadtree level-of-detail rendering system. Through extensive use of Unity's Job System and Burst compilation, the simulation achieves performance suitable for VR's demanding frame rate requirements. The system features a six-stage parallel simulation pipeline with inline twiddle factor computation, stack-allocated FFT buffers, Hermitian conjugate packing for SIMD-optimized temporal evolution, and an adaptive quadtree with 16 pre-computed edge-stitching configurations. This document focuses exclusively on the core mathematical foundations, algorithmic details, and parallel architecture that constitute the simulation engine.

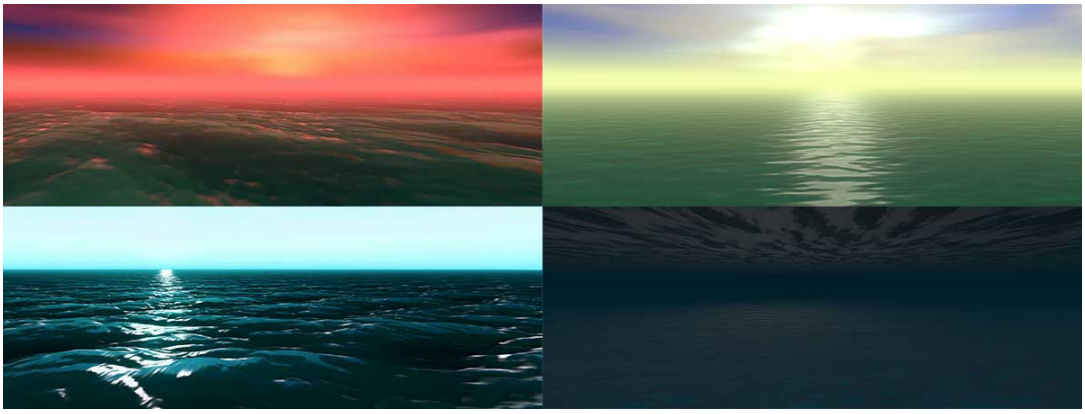

1 Introduction

Real-time ocean simulation remains a challenging problem in computer graphics, particularly for virtual reality where maintaining high frame rates with stereoscopic rendering is crucial for user comfort. This work presents a solution that balances visual quality with computational efficiency through parallel processing and adaptive rendering techniques. The simulation builds upon Tessendorf's seminal work on ocean surface modeling (Tessendorf, 1999), implementing the Phillips spectrum for initial wave amplitude distribution and utilizing inverse Fast Fourier Transform (iFFT) for efficient wave synthesis. The core contributions of this implementation include:

- A six-stage parallelized simulation pipeline using Unity's Job System with Burst compilation, featuring inline twiddle factor computation and stack-allocated FFT buffers for optimal cache utilization
- Hermitian conjugate packing with algebraically derived SIMD pre-transformations that reduce the temporal evolution to a single vectorized multiply-add per wave vector
- An adaptive quadtree-based level-of-detail system with iterative stack-based traversal, 16 pre-computed edge-stitching index buffer configurations, and frustum-culled GPU instanced rendering
- A complete surface gradient pipeline computing normals via central differences, Jacobian-based foam detection, polynomial roughness-to-smoothness conversion, and RGBA8 channel packing with mipmap generation

2 Testing Environment and Hardware Requirements

2.1 Development Environment

The ocean simulation system was developed and optimized using Unity 6000.0.58f2, leveraging the latest performance improvements and rendering features of Unity 6. The implementation utilizes the Universal Render Pipeline (URP) 17.0.4 for optimal VR rendering performance.

2.2 Target Hardware Platform

The primary target platform is the Meta Quest 3, offering a Qualcomm Snapdragon XR2 Gen 2 processor, 8GB RAM, native resolution of 2064×2208 per eye, and 90Hz/120Hz refresh rate capability. The Quest 3's enhanced processing power enables real-time FFT calculations while maintaining comfortable VR frame rates.

2.3 Minimum System Requirements

For development and PC VR deployment: 8-core CPU with AVX2 support for Burst compilation, RTX 3070 or equivalent GPU, 16GB RAM minimum (32GB recommended for larger grids), Unity 6000.0.58f2 or later, and OpenXR 1.15.1 with Meta Quest support.

3 Mathematical Foundation

3.1 Ocean Wave Theory

The ocean surface simulation is based on the linear superposition of sinusoidal waves with different frequencies and directions. The height field $h(\mathbf{x}, t)$ at position $\mathbf{x} = (x, z)$ and time t is computed as the sum of complex amplitudes:

$$h(\mathbf{x}, t) = \sum_{\mathbf{k}} \tilde{h}(\mathbf{k}, t) e^{i\mathbf{k}\cdot\mathbf{x}} \tag{1}$$

where $\mathbf{k}$ represents the wave vector and $\tilde{h}(\mathbf{k}, t)$ is the time-dependent complex amplitude in frequency domain. The wave vectors are discretized on a regular grid of resolution $N \times N$:

$$\mathbf{k}_{m,n} = \frac{2\pi}{L_{\text{patch}}} \left(m - \frac{N}{2},\ n - \frac{N}{2} \right), \quad m, n \in \{0, \ldots, N-1\} \tag{2}$$

where L_{patch} is the physical extent of the ocean patch and $N \in \{16, 32, 64, 128, 256, 512\}$.

3.2 Phillips Spectrum

The initial wave spectrum follows the Phillips spectrum (Tessendorf, 1999), which describes the statistical distribution of ocean waves based on wind conditions.

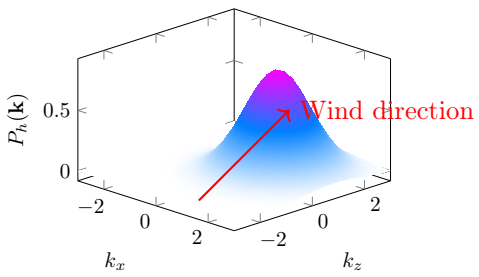

Figure 1: Phillips spectrum showing wave energy distribution in frequency space

The theoretical Phillips spectrum is given by:

$$P_h(\mathbf{k}) = A\frac{e^{-1/(kL)^2}}{k^4} \cdot D(\mathbf{k}, \hat{\mathbf{w}}) \tag{3}$$

where $k = |\mathbf{k}|$ is the wave number magnitude, $L = V^2/g$ is the largest wave scale (peak wavelength), V is the wind speed, g is gravitational acceleration, and $\hat{\mathbf{w}}$ is the normalized wind direction.

3.2.1 Amplitude Normalization

The practical implementation requires normalization factors to ensure energy conservation and FFT compatibility. The amplitude scale factor decomposes into two independent terms, an FFT resolution normalization and a spatial density normalization:

$$A = A_{\text{FFT}}^2 \cdot A_{\text{spatial}}^2 \tag{4}$$

where the individual factors are:

$$A_{\text{FFT}} = N^{-1/4}, \qquad A_{\text{spatial}} = \frac{e}{L_{\text{patch}}} \tag{5}$$

The FFT factor $N^{-1/4}$ compensates for the energy scaling inherent in the discrete Fourier transform: a transform of size N amplifies total energy by N, and the square root (from converting power spectrum to amplitude) yields $\sqrt{N}$. Taking the fourth root of the inverse produces the correct per-element normalization for the two-dimensional $N \times N$ grid. The spatial factor e/L_{patch} normalizes the energy density per unit area, where $e \approx 2.71828$ serves as a dimensionless scaling constant derived from the exponential decay characteristics of the spectrum.

3.2.2 Directional Spreading

The directional energy distribution uses a power-cosine spreading model. The spreading exponent is a quadratic function of the alignment parameter $\alpha \in [0, 1]$:

$$s(\alpha) = 1 + 5\alpha^2 \tag{6}$$

This maps $\alpha = 0$ (omnidirectional) to an exponent of 1, and $\alpha = 1$ (fully directional) to an exponent of 6. The directional factor applied to the spectrum is:

$$D(\mathbf{k}, \hat{\mathbf{w}}) = |\hat{\mathbf{k}} \cdot \hat{\mathbf{w}}|^s \tag{7}$$

where $\hat{\mathbf{k}} = \mathbf{k}/k$ is the normalized wave direction.

3.2.3 Counter-Wave Suppression

For waves traveling against the wind direction ($\hat{\mathbf{k}} \cdot \hat{\mathbf{w}} < 0$), an energy suppression factor models the physical dissipation of counter-propagating waves:

$$\sigma(\alpha) = 0.01 + 0.49(1 - \alpha)^2 \tag{8}$$

At full alignment ($\alpha = 1$), opposing waves retain only 1% of their energy; at no alignment ($\alpha = 0$), they retain 50%. The suppression enters the amplitude as a square root factor to operate in the amplitude domain rather than the power domain:

$$h_0^{\text{opposing}} = h_0 \cdot \sqrt{\sigma(\alpha)} \tag{9}$$

3.2.4 Small-Wave Suppression

To suppress small wavelengths that cause aliasing artifacts, an exponential Gaussian cutoff is applied in the frequency domain:

$$P'_h(\mathbf{k}) = P_h(\mathbf{k}) \cdot e^{-k^2 \, l_{\text{cutoff}}^2} \tag{10}$$

The cutoff wavelength l_{cutoff} is interpolated exponentially between bounds, providing logarithmically uniform control across the suppression range:

$$l_{\text{cutoff}} = l_{\min} \cdot \left(\frac{L_{\text{patch}} \cdot 0.25}{l_{\min}} \right)^{\beta} \tag{11}$$

with $l_{\min} = 0.001$, the upper bound at 25% of patch size, and $\beta \in [0, 1]$ controlling suppression strength. This exponential interpolation ensures that the parameter β produces perceptually uniform transitions: $\beta = 0$ applies virtually no suppression (cutoff at $l_{\min}$) while $\beta = 1$ aggressively filters all wavelengths below one quarter of the patch.

3.2.5 Stochastic Amplitude Generation

The initial complex amplitudes require Gaussian-distributed random variables. The Box-Muller transform converts uniform random samples $u_1, u_2 \sim \mathcal{U}(0, 1)$ into independent standard normal variates:

$$\begin{aligned} r &= \sqrt{-2 \ln u_1} \\ \xi_{\text{Re}} &= r \cdot \sin(2\pi u_2) \\ \xi_{\text{Im}} &= r \cdot \cos(2\pi u_2) \end{aligned} \tag{12}$$

The implementation generates four Gaussian values from four uniform inputs simultaneously, producing the two complex Gaussian variables ξ_+ and ξ_- needed for both the positive and negative frequency components in a single pass. Per-index deterministic seeding ensures reproducible spectra across frames and platforms.

```
[MethodImpl(MethodImplOptions.AggressiveInlining)]
private static float4 GenerateGaussianPair(float4 uniform) {
    var radius = sqrt(BOX_MULLER_RADIUS_SCALE * log(uniform.xz));
    var angle = TWO_PI * uniform.yw;

    return float4(
        radius.x * sin(angle.x),
        radius.x * cos(angle.x),
        radius.y * sin(angle.y),
        radius.y * cos(angle.y));
}
```

3.2.6 Complete Amplitude Computation

The final amplitude for spectral synthesis combines the spectrum magnitude with the stochastic component:

$$h_0(\mathbf{k}) = \frac{1}{\sqrt{2}}\,\xi \cdot \sqrt{P'_h(\mathbf{k}) \cdot D(\mathbf{k}, \hat{\mathbf{w}})} \tag{13}$$

where the $1/\sqrt{2}$ factor accounts for the Hermitian conjugate pairing: the total energy is distributed equally between $\tilde{h}_0(\mathbf{k})$ and $\tilde{h}_0^*(-\mathbf{k})$.

3.2.7 DC Component Guard

The spectrum has a singularity at $\mathbf{k} = (0, 0)$ where the wave number $k = 0$ causes division by zero in the k^{-4} term. This is handled by explicitly zeroing both the amplitude and angular frequency at the DC component before any computation:

$$h_0(\mathbf{0}) = 0, \qquad \omega(\mathbf{0}) = 0 \tag{14}$$

With this guard in place, the implementation uses fast floating-point mode with reduced precision across all jobs for maximum SIMD utilization.

3.3 Dispersion Relation

Ocean waves follow the deep-water dispersion relation linking angular frequency to wave number:

$$\omega(k) = \sqrt{g\,k} \tag{15}$$

For seamless tiling of the ocean animation, the continuous frequency is quantized to integer multiples of a fundamental frequency ω_0:

$$\omega'(k) = \left\lfloor \frac{\omega(k)}{\omega_0} \right\rfloor \omega_0, \qquad \omega_0 = \frac{2\pi}{T} \tag{16}$$

where T is the repeat period (configurable, default 200 seconds). This quantization ensures that all frequency components return to their initial phase after exactly T seconds, producing a seamlessly looping animation. The floor operation snaps each component to the nearest lower harmonic, introducing negligible visual error while guaranteeing periodicity.

3.4 Time Evolution and Hermitian Conjugate Packing

3.4.1 Theoretical Time Evolution

The time-dependent complex amplitudes evolve according to the dispersion relation:

$$\tilde{h}(\mathbf{k}, t) = \tilde{h}_0(\mathbf{k})\, e^{i\omega' t} + \tilde{h}_0^*(-\mathbf{k})\, e^{-i\omega' t} \tag{17}$$

This formulation guarantees a real-valued height field, as required physically. A naïve implementation would require accessing both index $\mathbf{k}$ and its conjugate $-\mathbf{k}$ for each evaluation, causing scattered memory access patterns that defeat cache prefetching.

3.4.2 Packed Representation

The implementation eliminates the conjugate index lookup by pre-computing and packing both components into a single four-component vector during spectrum generation. Define:

$$\mathbf{S}(\mathbf{k}) = \begin{pmatrix} \mathrm{Re}(\tilde{h}_0(\mathbf{k})) \\ \mathrm{Im}(\tilde{h}_0(\mathbf{k})) \\ \mathrm{Re}(\tilde{h}_0^*(-\mathbf{k})) \\ \mathrm{Im}(\tilde{h}_0^*(-\mathbf{k})) \end{pmatrix} = \begin{pmatrix} a \\ b \\ c \\ d \end{pmatrix} \tag{18}$$

This packing reduces memory bandwidth by 50% and enables purely sequential access patterns during time evolution.

3.4.3 SIMD Pre-Transformation Derivation

To reduce the time evolution to a single vectorized operation, the packed spectrum undergoes an algebraic pre-transformation during spectrum generation. Expanding the theoretical evolution:

$$\begin{aligned} \tilde{h}(\mathbf{k}, t) &= (a + bi)(\cos\phi + i\sin\phi) + (c + di)(\cos\phi - i\sin\phi) \\ &= \big[(a + c)\cos\phi + (d - b)\sin\phi\big] \\ &\quad + i\big[(b + d)\cos\phi + (a - c)\sin\phi\big] \\ &\text{where } \phi = \omega' t \end{aligned} \tag{19}$$

Defining the rotation vector $\mathbf{r} = (\cos\phi, \sin\phi)$, the goal is to express this as $\mathbf{S}'_{xy} \cdot r_x + \mathbf{S}'_{zw} \cdot r_y$ for some pre-transformed vector $\mathbf{S}'$. Collecting coefficients of $\cos\phi$ and $\sin\phi$:

$$\tilde{h} = \underbrace{\begin{pmatrix} a + c \\ b + d \end{pmatrix}}_{\mathbf{S}'_{xy}} \cos\phi + \underbrace{\begin{pmatrix} d - b \\ a - c \end{pmatrix}}_{\mathbf{S}'_{zw}} \sin\phi \tag{20}$$

The pre-transformation that produces these components from the original packing $\mathbf{S} = (a, b, c, d)$ is performed in two steps. First, construct the intermediate vector:

$$\mathbf{S}^{(1)} = \underbrace{(a, b, a, b)}_{\mathbf{S}_{xyxy}} + \underbrace{(c, d, -c, -d)}_{(\mathbf{S}_{zw}, -\mathbf{S}_{zw})} = (a{+}c,\ b{+}d,\ a{-}c,\ b{-}d) \tag{21}$$

Then swap and negate the zw components:

$$\mathbf{S}' = \big(S_x^{(1)},\ S_y^{(1)},\ S_w^{(1)},\ -S_z^{(1)}\big) = (a{+}c,\ b{+}d,\ b{-}d,\ c{-}a) \tag{22}$$

Verification. Substituting into $\mathbf{S}'_{xy} \cdot r_x + \mathbf{S}'_{zw} \cdot r_y$:

$$\begin{aligned} \mathrm{Re}(\tilde{h}) &= (a{+}c)\cos\phi + (b{-}d)\sin\phi \\ \mathrm{Im}(\tilde{h}) &= (b{+}d)\cos\phi + (c{-}a)\sin\phi \end{aligned} \tag{23}$$

Note that $b{-}d = -(d{-}b)$ and $c{-}a = -(a{-}c)$, which are the negated forms of the $\sin\phi$ coefficients from equation (19). This sign difference is absorbed by the pre-transformation structure: the swap-and-negate in equation (22) produces the complementary signs required for the $\mathbf{S}'_{zw} \cdot \sin\phi$ formulation. The temporal evolution thus reduces to:

$$\boxed{\tilde{h}(\mathbf{k}, t) = \mathbf{S}'_{xy}\cos(\omega' t) + \mathbf{S}'_{zw}\sin(\omega' t)} \tag{24}$$

Both trigonometric values are computed from a single intrinsic call, and the entire operation maps to one fused multiply-add on SIMD hardware.

```
public void Execute(int index) {
    var omega = _angularFrequencyTable[index];
    var phase = omega * _tim

    float2 rotation;
    sincos(phase, out rotation.y, out rotation.x

    var h0 = _initialAmplitudes[index];
    var heightSample = h0.xy * rotation.x + h0.zw * rotation.y;
    _heightSpectrum[index] = heightSampl

    var gridX = index & _indexMask;
    var gridY = index >> _logResolution;
    var waveVector = float2(gridX, gridY) - _halfResolutio

    var lengthSquared = dot(waveVector, waveVector);
    waveVector *= rsqrt(max(1.0f, lengthSquared)

    var heightConjugate = Conjugate(float2(heightSample.y, heightSample.x));
    var displacementX = heightConjugate * waveVector.x;
    var displacementZ = heightConjugate * waveVector.
    _displacementSpectrum[index] = float4(displacementX, displacementZ);
}
```

3.5 Displacement Calculation

3.5.1 Displacement Theory

The horizontal displacement for choppy waves is computed from the height spectrum using the normalized wave vector as a directional weight:

$$\mathbf{D}(\mathbf{x}, t) = -\lambda \sum_{\mathbf{k}} i \frac{\mathbf{k}}{k} \tilde{h}(\mathbf{k}, t)\, e^{i\mathbf{k}\cdot\mathbf{x}} \tag{25}$$

where $\lambda \in [0, 1]$ is the choppiness parameter controlling wave sharpness. The factor $i \cdot \mathbf{k}/k$ applies a 90° phase rotation scaled by the wave direction, concentrating surface area at wave crests and expanding it at troughs.

3.5.2 Bitwise Wave Vector Extraction

For a flattened linear index into the $N \times N$ grid, the two-dimensional grid coordinates are recovered without division or modulo using bitwise operations that exploit the power-of-two grid size:

$$\begin{aligned} g_x &= \texttt{index} \,\&\, (N-1) \\ g_y &= \texttt{index} \gg \log_2 N \end{aligned} \tag{26}$$

where & denotes bitwise AND and $\gg$ denotes right shift. The mask $(N-1)$ isolates the lower $\log_2 N$ bits (equivalent to $\bmod N$), while the shift extracts the upper bits (equivalent to $\lfloor \text{index}/N \rfloor$). The centered wave vector is then:

$$\mathbf{k}_{\text{grid}} = (g_x, g_y) - N/2 \tag{27}$$

3.5.3 Wave Vector Normalization

The wave direction $\hat{\mathbf{k}} = \mathbf{k}/|\mathbf{k}|$ uses reciprocal square root with a DC-safe guard:

$$\hat{\mathbf{k}} = \mathbf{k}_{\text{grid}} \cdot \text{rsqrt}\big(\max(1,\ |\mathbf{k}_{\text{grid}}|^2)\big) \tag{28}$$

The $\max(1, \cdot)$ clamp prevents division by zero at the origin while leaving all non-DC components unaffected (since $|\mathbf{k}|^2 \geq 1$ for all non-zero integer grid coordinates).

3.5.4 Vectorized Complex Displacement

The multiplication by the imaginary unit i performs a 90° phase rotation, which algebraically amounts to swapping and negating components of the complex number:

$$i \cdot (h_x + ih_y) = -h_y + ih_x \tag{29}$$

In the implementation, this is expressed as a conjugation with swapped input ordering: $\text{conj}(h_y, h_x) = (h_y, -h_x)$. The complete displacement computation for both horizontal axes is then vectorized into a single four-component operation:

$$\mathbf{D}_{\text{spec}} = \text{conj}(h_y, h_x) \otimes (\hat{k}_x, \hat{k}_x, \hat{k}_y, \hat{k}_y) \tag{30}$$

where $\otimes$ denotes element-wise multiplication and the subscript patterns indicate component replication. This produces both the x- and z-displacement spectra in a single SIMD instruction.

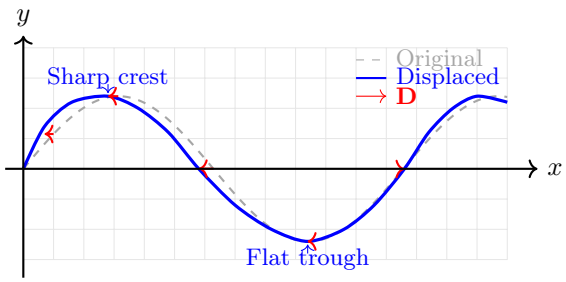

Figure 2: Horizontal displacement creating characteristic ocean wave profile with sharp crests and flat troughs

3.6 FFT Implementation

3.6.1 Discrete Fourier Transform

The summations in equation (1) are efficiently computed using the 2D inverse FFT. The one-dimensional DFT of N elements is:

$$X_k = \sum_{n=0}^{N-1} x_n \cdot W_N^{kn}, \qquad W_N = e^{-2\pi i/N} \tag{31}$$

where W_N is the primitive N-th root of unity. The 2D transform is computed as separable row-wise and column-wise 1D transforms.

3.6.2 Cooley-Tukey Butterfly Structure

The radix-2 decimation-in-time Cooley-Tukey algorithm (Cooley and Tukey, 1965) decomposes the DFT into $\log_2 N$ stages of $N/2$ butterfly operations each. At stage $p \in \{0, \ldots, \log_2 N - 1\}$, each butterfly operates on a pair of elements separated by stride 2^p:

$$\begin{aligned} X_{\text{top}} &= x_a + W_N^{k_t} \cdot x_b \\ X_{\text{bot}} &= x_a - W_N^{k_t} \cdot x_b \end{aligned} \tag{32}$$

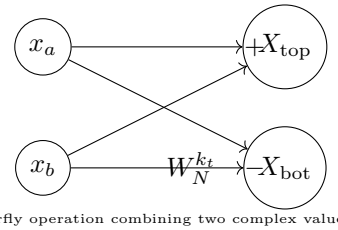

Figure 3: FFT butterfly operation combining two complex values with twiddle factor

3.6.3 Inline Twiddle Factor Computation

Rather than pre-computing and storing a butterfly lookup table, the twiddle factors are computed inline using Euler's formula:

$$W_N^{k_t} = e^{-2\pi i\, k_t/N} = \cos\left(\frac{-2\pi k_t}{N}\right) + i \sin\left(\frac{-2\pi k_t}{N}\right) \tag{33}$$

The twiddle exponent k_t for butterfly index j at stage p is derived from the butterfly's position within its group:

$$k_t = \underbrace{(j \bmod 2^p)}_{\text{position in group}} \cdot \underbrace{\frac{N}{2^{p+1}}}_{\text{inter-group spacing}} \tag{34}$$

The element indices for the butterfly pair are computed as:

$$\begin{aligned} g &= \lfloor j/2^p \rfloor && \text{(group index)} \\ \text{idx}_a &= g \cdot 2^{p+1} + (j \bmod 2^p) && \text{(top element)} \\ \text{idx}_b &= \text{idx}_a + 2^p && \text{(bottom element)} \end{aligned} \tag{35}$$

This approach trades additional ALU operations per butterfly for eliminated memory accesses to lookup tables, which is favorable on modern hardware where arithmetic throughput exceeds memory bandwidth. The trigonometric pair is computed with a single intrinsic call.

```
var group = butterfly / stride;
var posInGroup = butterfly % stride;

var idxA = group * (stride << 1) + posInGroup;
var idxB = idxA + stride;

var twiddleExponent = posInGroup * (_resolution >> (pass + 1));
var twiddle = TwiddleFactor(twiddleExponent, _resolution);

var hA = heightLocal[idxA];
var hB = heightLocal[idxB];
var hBTwiddle = Multiply(hB, twiddle);
heightTemp[idxA] = hA + hBTwiddle;
heightTemp[idxB] = hA - hBTwiddle;
```

3.6.4 Bit-Reversal Permutation

The decimation-in-time Cooley-Tukey algorithm requires input data in bit-reversed order. For an index i with $b = \log_2 N$ significant bits, the bit-reversed index is:

$$\text{BitReverse}(i, b) = \text{reversebits}(i) \gg (32 - b) \tag{36}$$

where reversebits is a hardware intrinsic that reverses all 32 bits of an unsigned integer, and the right shift discards the $(32 - b)$ least significant bits of the reversed result. For example, with $N = 8$ ($b = 3$):

$$\begin{aligned} \text{BitReverse}(1, 3): &\quad 001_2 \xrightarrow{\text{rev32}} \ldots 100_2 \xrightarrow{\gg 29} 100_2 = 4 \\ \text{BitReverse}(3, 3): &\quad 011_2 \xrightarrow{\text{rev32}} \ldots 110_2 \xrightarrow{\gg 29} 110_2 = 6 \end{aligned} \tag{37}$$

This produces the standard input ordering: $\{x_0, x_4, x_2, x_6, x_1, x_5, x_3, x_7\}$ for $N = 8$.

3.6.5 Stack-Allocated Buffer Strategy

The FFT implementation avoids persistent heap-allocated ping-pong buffers by using stack-allocated memory for each row or column. Each parallel work item allocates four local buffers:

$$\text{Buffers} = \begin{cases} \texttt{local}_h[N],\ \texttt{local}_d[N] & \text{primary working buffers} \\ \texttt{temp}_h[N],\ \texttt{temp}_d[N] & \text{swap targets per stage} \end{cases} \tag{38}$$

where subscripts h and d denote height (2-component) and displacement (4-component) data respectively. Both spectra are processed in the same job to maximize data reuse. The data flow for a single FFT work item proceeds in three phases:

1. **Load**: Input data is gathered from global arrays with bit-reversed indexing into the local buffers
2. **Compute**: All $\log_2 N$ butterfly stages are processed entirely in local memory, with buffer references swapped (pointer swap, zero copy) after each stage
3. **Store**: The final result is written back to global output arrays in a single sequential pass

This strategy provides two critical advantages. First, stack memory resides in L1 cache throughout the computation, eliminating cache misses during the iterative butterfly stages. Second, no

persistent buffer management is needed between frames since the allocations are automatically reclaimed when the work item completes.

3.6.6 Dual-Spectrum Processing

The horizontal and vertical FFT passes simultaneously transform both the height spectrum (stored as 2-component complex values) and the displacement spectrum (stored as 4-component values encoding both x- and z-displacement as complex pairs). Each butterfly operation is applied to both spectra using the same twiddle factor:

$$\begin{aligned} h_{\text{top}} &= h_a + \text{Mul}(h_b, W), \qquad d_{\text{top}} = d_a + \big(\text{Mul}(d_b^{xy}, W),\ \text{Mul}(d_b^{zw}, W)\big) \\ h_{\text{bot}} &= h_a - \text{Mul}(h_b, W), \qquad d_{\text{bot}} = d_a - \big(\text{Mul}(d_b^{xy}, W),\ \text{Mul}(d_b^{zw}, W)\big) \end{aligned} \tag{39}$$

where $\text{Mul}(a, b) = (a_x b_x - a_y b_y,\ a_x b_y + a_y b_x)$ is the complex multiplication. This co-processing eliminates redundant twiddle factor computation and exploits instruction-level parallelism.

3.6.7 Vertical Pass Memory Access Pattern

The horizontal pass operates on contiguous rows, achieving optimal sequential access. The vertical pass must gather column data from strided memory (stride = N elements). The implementation loads strided input into contiguous stack-allocated buffers before processing:

$$\texttt{local}[r] = \texttt{source}[\text{col} + \text{BitReverse}(r, b) \cdot N], \quad r \in \{0, \ldots, N{-}1\} \tag{40}$$

After the FFT, results are scattered back with the transpose:

$$\texttt{result}[\text{col} + r \cdot N] = \texttt{local}[r] \tag{41}$$

This gather-process-scatter pattern converts the unfavorable column access into sequential local processing, allowing the L1 cache to serve the butterfly stages without cache line thrashing.

3.7 Displacement Finalization

After the 2D FFT, the raw frequency-domain output requires two corrections to produce the final spatial-domain displacement field.

3.7.1 Sign Correction

The standard DFT convention places the DC component at index $(0, 0)$, but the centered spectrum representation (with $\mathbf{k}$ offset by $N/2$) introduces an alternating sign pattern that must be corrected:

$$s(x, y) = (-1)^{x+y} \tag{42}$$

This is computed branch-free using a bitwise test:

$$s = \begin{cases} +1 & \text{if } (x + y)\ \&\ 1 = 0 \\ -1 & \text{otherwise} \end{cases} \tag{43}$$

3.7.2 Final Displacement Assembly

The sign correction and choppiness scaling are combined in a single pass:

$$\mathbf{D}_{\text{final}}(x, y) = \big(-D_x \cdot \lambda \cdot s,\ \ h \cdot s,\ \ -D_z \cdot \lambda \cdot s\big) \tag{44}$$

where h is the height from the FFT output, D_x, D_z are the horizontal displacement components, λ is the choppiness parameter, and s is the sign correction. The output is dual-written to both a three-component floating-point array (for subsequent gradient computation) and a four-component half-precision texture array (for GPU rendering), avoiding a separate copy pass.

3.8 Surface Gradient Computation

3.8.1 Normal Calculation via Central Differences

Surface normals are computed from the displacement field using central finite differences with toroidal (wrap-around) boundary conditions:

$$\left.\frac{\partial \mathbf{D}}{\partial x}\right|_{c,r} \approx \frac{\mathbf{D}(c{+}1, r) - \mathbf{D}(c{-}1, r)}{2} \cdot \frac{N}{L_{\text{patch}}} \tag{45}$$

The factor N/L_{patch} converts from texel-space differences to world-space derivatives. Indices wrap toroidally:

$$\text{wrap}(i) = (i + N) \bmod N \tag{46}$$

The surface normal is constructed from the height derivatives:

$$\mathbf{n} = \text{normalize}\left(-\frac{\partial h}{\partial x},\ 1,\ -\frac{\partial h}{\partial z}\right) \tag{47}$$

3.8.2 Jacobian Determinant for Foam Detection

Wave breaking is detected through the Jacobian determinant of the displaced surface mapping. When the horizontal displacement causes the surface to fold (multiple surface points mapping to the same horizontal position), the Jacobian becomes negative:

$$J = \underbrace{\left(1 + \frac{\partial D_x}{\partial x}\right)}_{J_{xx}} \underbrace{\left(1 + \frac{\partial D_z}{\partial z}\right)}_{J_{zz}} - \underbrace{\frac{\partial D_x}{\partial z}}_{J_{xz}} \underbrace{\frac{\partial D_z}{\partial x}}_{J_{zx}} \tag{48}$$

When $J < 0$, the surface has folded and foam should appear. When $J > 0$, the surface is smooth. The threshold $J = 0$ marks the exact breaking point. This determinant is stored in the blue channel of the output texture for use by the rendering shader.

3.8.3 Roughness-to-Normal-Length Polynomial

To encode surface roughness information into the normal map for physically correct mipmap filtering, the implementation maps material roughness $r \in [0, 1]$ to an expected normal vector length using a polynomial approximation of the microfacet distribution integral:

$$|\mathbf{n}|_{\text{scaled}} = 1 - r\big(0.306 + r(0.113 + r \cdot 0.081)\big) \tag{49}$$

This Horner-form polynomial requires exactly 3 fused multiply-add (FMA) operations with no branches or transcendental functions. The approximation maps $r = 0$ (perfectly smooth) to $|\mathbf{n}| = 1$ and $r = 1$ (maximum roughness) to $|\mathbf{n}| = 0.5$. The coefficients were fitted to replace the expensive atanh-based conversion from Beckmann microfacet theory.

3.8.4 RGBA8 Channel Packing

The surface gradient data is packed into a 32-bit integer for direct texture upload. The normal vector components are mapped from the signed range $[-1, 1]$ to unsigned $[0, 1]$, then quantized to 8-bit integers:

$$\begin{aligned} R &= \lfloor (n_x \cdot 0.5 + 0.5) \cdot 255 + 0.5 \rfloor \\ G &= \lfloor (n_z \cdot 0.5 + 0.5) \cdot 255 + 0.5 \rfloor \\ B &= \lfloor \text{saturate}(J \cdot 0.5 + 0.5) \cdot 255 + 0.5 \rfloor \\ A &= \lfloor \text{smoothness} \cdot 255 + 0.5 \rfloor \end{aligned} \tag{50}$$

The four bytes are combined into a single 32-bit integer using bit shifts:

$$\text{packed} = R \mid (G \ll 8) \mid (B \ll 16) \mid (A \ll 24) \tag{51}$$

where $\ll$ denotes left shift and $\mid$ denotes bitwise OR. This packing is performed identically in both the base-level gradient job and the mipmap filter jobs, ensuring consistent data layout across all mip levels.

3.9 Mipmap Generation

3.9.1 Box Filter Averaging

A chain of mipmap filter jobs generates the mipmap pyramid from the base-level normal and foam data. For each mip level m from 1 to $\log_2 N$, the four source texels are averaged:

$$\bar{\mathbf{n}}_m(x, y) = \frac{1}{4} \sum_{i=0}^{1} \sum_{j=0}^{1} \mathbf{n}_{m-1}(2x + i, 2y + j) \tag{52}$$

Critically, the averaged result preserves the *unnormalized* normal vectors. The length of the averaged normal encodes the variance of the source normals: when all four source normals point in the same direction, $|\bar{\mathbf{n}}| \approx 1$; when they diverge significantly, $|\bar{\mathbf{n}}| \ll 1$.

3.9.2 Normal-Length to Smoothness Conversion

The averaged normal length is converted to an equivalent smoothness value suitable for the rendering shader's roughness model. The conversion maps the domain $[2/3, 1]$ to $[0, 1]$ using a two-stage polynomial:

$$\begin{aligned} t &= \text{saturate}\left(\frac{|\bar{\mathbf{n}}| - 2/3}{1/3} \right) \\ r &= 1 - t(0.85 + 0.15t) \\ \text{smoothness} &= 1 - \sqrt{r} \end{aligned} \tag{53}$$

The first line normalizes the input to $[0, 1]$. The second line converts to roughness using a quadratic that transitions from $r = 1$ (maximum roughness) at $t = 0$ to $r = 0$ (perfectly smooth) at $t = 1$, with the coefficients 0.85 and 0.15 providing a slightly concave profile that matches perceptual roughness better than a linear ramp. The final square root converts from roughness to smoothness in the standard PBR convention where smoothness $= 1 - \sqrt{\text{roughness}}$.

After conversion, the averaged normal is re-normalized and packed into RGBA8 format using the same bit-packing scheme described in Section 3.8.4, with the smoothness value replacing the

base-level smoothness in the alpha channel.

4 Parallel Implementation

4.1 Job System Architecture

The ocean simulation leverages Unity's Job System with Burst compilation to achieve parallelization. The computation pipeline consists of a six-stage chain of specialized jobs, each compiled with reduced floating-point precision and fast math mode for maximum SIMD throughput. All safety checks are disabled in production to eliminate bounds checking overhead.

4.2 Pipeline Stages

4.2.1 Stage 1: Spectrum Generation

Computes the Phillips spectrum with directional spreading for all N^2 wave vectors as an embarrassingly parallel operation (one work item per wave vector, batch size 64). This stage simultaneously generates both the positive and negative frequency amplitudes, applies the SIMD pre-transformation derived in Section 3.4.3, and stores the result in the packed four-component representation (equation 18). This job runs **on demand**, only when wind parameters or profile change, not every frame.

4.2.2 Stage 2: Temporal Evolution

Advances all wave amplitudes forward in time using the packed SIMD formulation (equation 24). Each work item computes the trigonometric pair via a single intrinsic, performs the vectorized height evaluation, extracts the wave vector via bitwise operations (Section 3.5.2), and produces the displacement spectrum (equation 30). The operation is embarrassingly parallel with zero data dependencies between elements.

4.2.3 Stage 3–4: Separable 2D FFT

The horizontal pass (Stage 3) processes each of the N rows independently, and the vertical pass (Stage 4) processes each of the N columns independently. Both passes use the stack-allocated buffer strategy (Section 3.6.5) with bit-reversed input loading, $\log_2 N$ butterfly stages with inline twiddle computation (Section 3.6.3), and dual-spectrum processing (equation 39). The pipeline uses a double-buffering scheme: Stage 3 reads from buffer A and writes to buffer B; Stage 4 reads from buffer B and writes back to buffer A.

4.2.4 Stage 5: Displacement Finalization

Applies sign correction and choppiness scaling (equation 44), dual-writing the result to both the CPU-side displacement array and the GPU-side half-precision texture data.

4.2.5 Stage 6+: Surface Gradients and Mipmaps

Computes normals via central differences, the Jacobian determinant, roughness-scaled normal length, and RGBA8 packing (Section 3.8.3 through Section 3.8.4). Subsequently, a chain of $\log_2 N$ mipmap filter jobs generates the complete mip pyramid with per-level smoothness encoding.

4.3 Pipeline Scheduling and Double Buffering

All stages are scheduled as a dependency chain within a single frame:

$$\text{Handle}_n = \text{Job}_n.\text{Schedule}(\ldots,\ \text{Handle}_{n-1}) \tag{54}$$

The final call submits the entire chain to worker threads. Texture data is applied to GPU textures at the start of the *next* frame, allowing the CPU to proceed with other work while the jobs execute asynchronously.

The buffer flow through the FFT stages follows an A→B→A pattern:

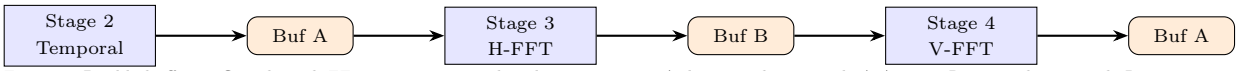

Figure 4: Double-buffering flow through FFT stages: temporal evolution writes to A, horizontal pass reads A / writes B, vertical pass reads B / writes A

Stage	Job	Parallel Strategy
1	WaveSpectrumInitializerJob	Per wave vector (on demand)
2	TemporalEvolutionJob	Per wave vector
3	HorizontalSpectralPassJob	Per row
4	VerticalSpectralPassJob	Per column
5	DisplacementFinalizationJob	Per pixel
6	SurfaceGradientJob	Per pixel
6+	MipmapFilterJob ($\times \log_2 N$)	Per mip pixel

Table 1: Six-stage simulation pipeline with parallelization strategy

All parallel jobs use a batch size of 64 elements, balancing scheduling overhead against work distribution granularity.

4.4 Mipmap Offset Computation

The mipmap chain is stored in a single contiguous pixel buffer. The write offset for mip level m within this buffer is computed from the geometric series of mip sizes:

$$\text{offset}(m) = \frac{4N^2 - 1}{3} - \frac{4^{(\log_2 N + 1 - m)} - 1}{3} \tag{55}$$

The first term is the total pixel count across all mip levels (the sum $N^2 + (N/2)^2 + \cdots + 1 = (4N^2 - 1)/3$). The second term subtracts the remaining pixels from level m onward, yielding the correct byte offset for contiguous storage.

5 Adaptive Quadtree Rendering

5.1 Hierarchical Level-of-Detail System

The ocean surface utilizes an adaptive quadtree structure to efficiently render vast water areas while maintaining geometric detail near the viewer. The system supports configurable quality

presets:

Preset	**Vertices** V	**LOD Scale** τ	**Cull Scale** β
Low	16	2.0	1.2
Medium	32	1.5	1.5
High	64	1.2	1.8
Ultra	64	1.0	2.0

Table 2: Quality presets controlling mesh density and LOD transitions

The maximum number of subdivision levels is computed automatically from the ocean size $S \in [256, 8192]$:

$$L_{\max} = \text{clamp}\left(\left\lfloor \log_2 \frac{S}{64} + 0.5 \right\rfloor,\ 2,\ 8\right) \tag{56}$$

This produces a subdivision map of width $W = 2^{L_{\max}}$ cells at the finest level.

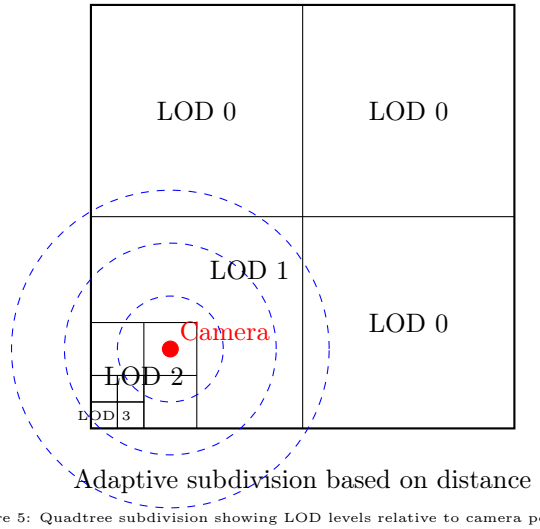

Figure 5: Quadtree subdivision showing LOD levels relative to camera position

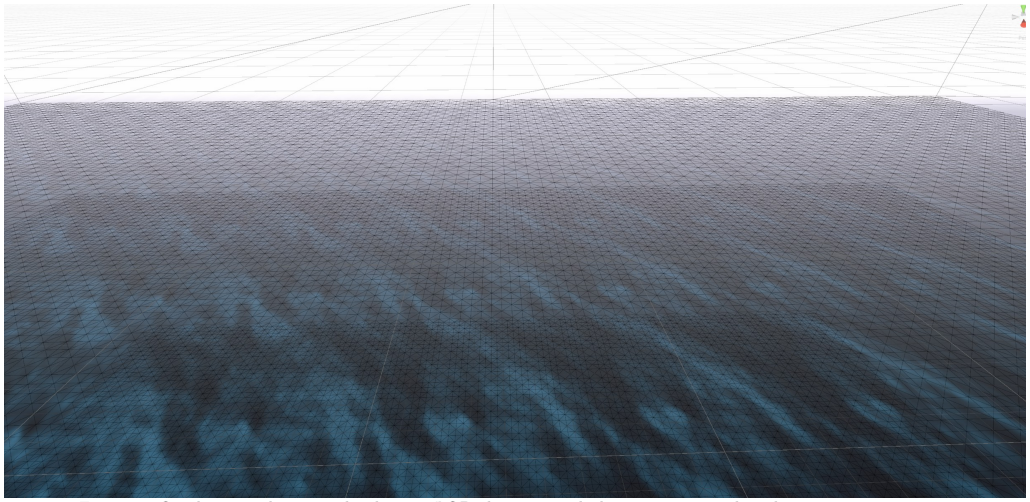

Figure 6: Quadtree rendering with adaptive LOD showing mesh density variation based on camera proximity

5.2 Iterative Quadtree Traversal

The quadtree traversal is implemented as a single-threaded Burst-compiled job using an explicit stack rather than recursion, ensuring deterministic performance. The traversal maintains a stack of node descriptors, each storing grid coordinates (x, y), subdivision level, LOD level, and a rendered flag (Pajarola, 2002).

5.2.1 Traversal Algorithm

The algorithm begins with the root node at level 0 covering the entire ocean. For each node popped from the stack, the subdivision decision is based on a squared-distance comparison:

$$\text{subdivide} = |\mathbf{c}_{\text{node}} - \mathbf{p}_{\text{viewer}}|^2 < (s_{\text{node}} \cdot \tau)^2 \tag{57}$$

where $\mathbf{c}_{\text{node}}$ is the node center in world space, $s_{\text{node}} = S/2^l$ is the node size at level l, and τ is the LOD distance scale from the quality preset. Both sides use squared quantities to avoid a square root.
The node center is reconstructed from grid coordinates:

$$\mathbf{c}_{\text{node}} = \mathbf{c}_{\text{grid}} - \frac{S}{2}\hat{\mathbf{1}} + (x + 0.5,\ 0,\ y + 0.5) \cdot s_{\text{node}} \tag{58}$$

The processing logic follows three rules:

1. If the node should *not* subdivide and has not been rendered by an ancestor: attempt frustum-culled rendering
2. If the node is not at leaf level: push four children onto the stack (in reverse order to process lower-left first)
3. At leaf level: write the LOD value to the subdivision map and render if not yet handled

The `HasRendered` flag propagates from parent to children, preventing double-rendering when a coarser ancestor has already emitted the patch. Children inherit the rendered state via $\texttt{childRendered} = \texttt{parentRendered} \vee (\neg\texttt{subdivide} \wedge \texttt{visible})$.

5.2.2 Frustum Culling

Each node is tested against the six camera frustum planes using an AABB (Axis-Aligned Bounding Box) test. For each plane with normal $\mathbf{n}$ and distance d, the *positive vertex* (the corner farthest in the direction of the normal) is tested:

$$\mathbf{p}_{\text{test}} = \mathbf{c} + \text{select}(-\mathbf{e}, \mathbf{e}, \mathbf{n} \geq 0) \tag{59}$$

where $\mathbf{c}$ is the box center, $\mathbf{e}$ the half-extents, and select is a component-wise conditional. The node is visible only if:

$$\mathbf{n} \cdot \mathbf{p}_{\text{test}} + d \geq 0 \quad \text{for all 6 planes} \tag{60}$$

The bounding box extents account for maximum possible wave displacement:

$$\mathbf{e} = \left(\frac{s \cdot \beta}{2},\ \frac{h_{\max}}{2},\ \frac{s \cdot \beta}{2} \right) \tag{61}$$

where β is the cull scale preset and $h_{\max}$ is the maximum expected displacement height (computed as $S \cdot 0.03$ by default or user-overridden).

5.3 Edge Stitching for Crack Prevention

Adjacent quadtree nodes at different LOD levels create T-junctions where the finer mesh has vertices along an edge that do not exist in the coarser neighbor. These T-junctions manifest as visible cracks in the rendered surface.

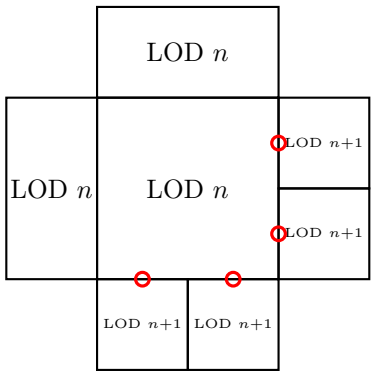

T-junctions requiring edge stitching

Figure 7: T-junction formation at LOD boundaries

5.3.1 Neighbor Detection and Stride Computation

For each visible patch at grid position (x, y) and level l, the neighbor LOD levels are read from the subdivision map. The stride at the current level determines where to sample neighbors:

$$\Delta = 2^{(L_{\max} - l)} \tag{62}$$

Neighbor positions in the finest-level map are:

$$\begin{aligned} \text{East}: &\quad (g_x + \Delta,\ g_y) \\ \text{West}: &\quad (g_x - 1,\ g_y) \\ \text{North}: &\quad (g_x,\ g_y + \Delta) \\ \text{South}: &\quad (g_x,\ g_y - 1) \end{aligned} \tag{63}$$

where $g_x = x \cdot \Delta$ and $g_y = y \cdot \Delta$ are the map-space coordinates. Neighbors outside the map bounds are treated as having the same LOD (no stitching needed).

5.3.2 Edge Configuration Flags

Each edge direction is encoded as a single bit in a 4-bit flag word:

$$\text{flags} = \sum_{d \in \{\text{E,N,W,S}\}} 2^{f(d)} \cdot [\text{LOD}_d < l] \tag{64}$$

where $f(\text{E}) = 0$, $f(\text{N}) = 1$, $f(\text{W}) = 2$, $f(\text{S}) = 3$, and $[\cdot]$ is the Iverson bracket evaluating to 1 when the neighbor has a coarser (numerically lower) LOD level. This produces a value in $\{0, \ldots, 15\}$ that uniquely identifies one of the 16 possible edge-stitching configurations.

```
var stride = 1 << (LodLevels - lod);
var gx = patchX * stride;
var gy = patchY * stride;

var width = MapWidt

var flags = AdjacentLodFlags.None;
flags |= GetNeighborFlag(gx + stride, gy, width, lod, AdjacentLodFlags.East);
flags |= GetNeighborFlag(gx - 1, gy, width, lod, AdjacentLodFlags.West);
flags |= GetNeighborFlag(gx, gy + stride, width, lod, AdjacentLodFlags.North);
flags |= GetNeighborFlag(gx, gy - 1, width, lod, AdjacentLodFlags.South);
```

5.3.3 Triangulation Patterns

Each patch is divided into a grid of $V/2 \times V/2$ cells, where each cell corresponds to a 3×3 vertex sub-grid

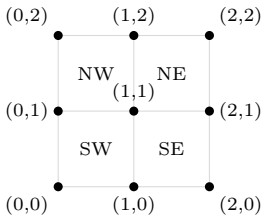

Figure 8: Cell vertex layout for edge-stitching triangulation patterns

Only cells along patch boundaries receive edge-specific flags; interior cells always use the full 8-triangle pattern (flags = 0). The flag for a specific cell is determined by its position within the patch:

$$\text{cellFlags} = \begin{cases} \texttt{West} & \text{if } x = 0 \text{ and patchFlags has West} \\ \texttt{East} & \text{if } x = V/2 - 1 \text{ and patchFlags has East} \\ \quad\vdots & \text{(analogous for North, South)} \end{cases} \tag{65}$$

The 16 triangulation patterns range from the full 8-triangle subdivision (no coarser neighbors) to the minimal 4-triangle fan (all four neighbors coarser):

$$\begin{aligned} \text{flags} = 0000_2 &: \quad 8 \text{ triangles (full detail)} \\ \text{flags} = 0001_2 &: \quad 7 \text{ triangles (East edge merged)} \\ &\vdots \\ \text{flags} = 1111_2 &: \quad 4 \text{ triangles (corner fan)} \end{aligned} \tag{66}$$

When an edge is marked for stitching, the midpoint vertex along that edge is omitted from the triangulation, and the adjacent triangles are replaced with a fan that connects directly to the corner vertices. This ensures that the shared edge between adjacent patches at different LOD levels has identical vertex positions, eliminating T-junction cracks.

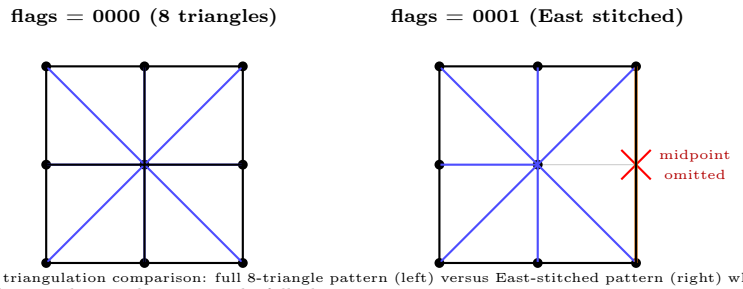

Figure 9: Edge-stitching triangulation comparison: full 8-triangle pattern (left) versus East-stitched pattern (right) where the midpoint vertex is omitted and replaced by a single triangle spanning the full edge

5.4 Mesh Generation

Each LOD level uses a regular grid mesh with $(V+1) \times (V+1)$ vertices in unit space $[-0.5, 0.5]^2$:

$$\mathbf{v}_{i,j} = \left(\frac{i}{V} - 0.5,\ \ 0,\ \ \frac{j}{V} - 0.5 \right), \quad i, j \in \{0, \ldots, V\} \tag{67}$$

The mesh is created with 16 submeshes (one per edge configuration). Each submesh's index buffer is generated by iterating over the $V/2 \times V/2$ cell grid, determining the per-cell flags (equation 65), and emitting the corresponding triangle pattern. The vertex index for triangle vertex (v_x, v_y) in cell (c_x, c_y) within the $(V+1) \times (V+1)$ grid is:

$$\text{idx} = (2c_x + v_x) + (2c_y + v_y) \cdot (V + 1) \tag{68}$$

5.5 Grid Snapping

To prevent swimming artifacts during camera movement, the grid origin snaps to discrete cell positions:

$$\mathbf{c}_{\text{snap}} = \left\lfloor \frac{\mathbf{c}_{\text{camera}}}{\delta} \right\rfloor \cdot \delta, \qquad \delta = \frac{S}{2V} \tag{69}$$

The snap cell size δ is chosen such that vertices align across adjacent LOD boundaries. Since each coarser level has exactly twice the cell size, the finest-level cell size guarantees alignment at all levels. The snap operates independently on the x and z axes.

5.6 Instance Batching

Patches sharing the same edge configuration are rendered using GPU instancing to minimize draw calls. The renderer maintains 16 transformation matrix arrays, one per submesh configuration:

$$\mathbf{M}_{\text{instance}} = \text{TRS}(\mathbf{c}_{\text{patch}},\ \mathbf{I},\ s_{\text{patch}}) \tag{70}$$

where $\mathbf{c}_{\text{patch}}$ is the world-space patch center (computed from grid position, level, and snapped center), $\mathbf{I}$ is the identity rotation, and $s_{\text{patch}} = S/2^l$ is the uniform scale for level l. The maximum batch size is capped at 128 instances per draw call, yielding at most $16 \times 1 = 16$ instanced draw calls per camera, a reduction from potentially hundreds of individual draw calls.

5.7 Skirting Mesh

For horizon rendering beyond the main quadtree grid, a strip mesh extends from the ocean boundary to a configurable distance (default $10 \times S$). The mesh consists of 3 vertex pairs forming a triangle strip from inner extent $S/2$ to outer extent. Four instances are rendered per camera,

oriented along the cardinal directions, providing a continuous horizon without additional LOD overhead.

References

Cooley, James W. and John W. Tukey (1965). "An algorithm for the machine calculation of complex Fourier series". In: *Mathematics of Computation* 19.90, pp. 297–301. ISSN: 0025-5718, 1088-6842. DOI: 10.1090/S0025-5718-1965-0178586-1. URL: https://www.ams.org/mcom/1965-19-090/S0025-5718-1965-0178586-1/ (visited on 05/07/2025).

Pajarola, Renato (2002). "Overview of quadtree-based terrain triangulation and visualization". In: URL: https://escholarship.org/uc/item/24h2g848 (visited on 03/05/2025).

Tessendorf, Jerry (1999). *Simulating Ocean Water*. URL: https://evasion.inrialpes.fr/Membres/Fabrice.Neyret/NaturalScenes/fluids/water/waves/fluids-nuages/waves/Jonathan/articlesCG/simulating-ocean-water-01.pdf (visited on 05/18/2025).